Deposition of CdS, CdS/ZnSe and CdS/ZnSe/ZnS shells around CdSeTe alloyed core quantum dots: Effects on optical properties

Oluwasesan Adegoke[a], Tebello Nyokong[b], Patricia B.C. Forbes[a] *

[a]*Department of Chemistry, Faculty of Natural and Agricultural Sciences, University of Pretoria, Lynnwood Road, Pretoria 0002, South Africa*
[b]*Department of Chemistry, Rhodes University, Grahamstown 6140, South Africa*

Abstract

In this work, we have synthesized water-soluble L-cysteine-capped alloyed CdSeTe core QDs and investigated the structural and optical properties of deposition of each of CdS, CdS/ZnSe and CdS/ZnSe/ZnS shell layers. Photophysical results showed that the overcoating of a CdS shell around the alloyed CdSeTe core (QY = 8.4%) resulted in an effective confinement of the radiative exciton with an improved QY value of 93.5%. Subsequent deposition of a ZnSe shell around the CdSeTe/CdS surface decreased the QY to 24.7% but an increase in the QY value of up to 49.5% was observed when a ZnS shell was overcoated around the CdSeTe/CdS/ZnSe surface. QDs with shell layers showed improved stability relative to the core. Data obtained from time-resolved fluorescence measurements provided useful insight into the variations in the photophysical properties of the QDs upon the formation of each shell layer. Our study suggests that the formation of the CdSeTe/CdS core/shell QDs meets the requirements of quality QDs in terms of high PL QY and stability, hence further deposition of additional shells are not necessary in improving the optical properties of the core/shell QDs.

Keywords: Alloys; nanostructures; semiconductor; photoluminescence; quantum dots

*Corresponding author:
Email address: adegoke.sesan@mailbox.co.za (O. Adegoke), t.nyokong@ru.ac.za (T. Nyokong), patricia.forbes@up.ac.za (P.B.C. Forbes)

1. Introduction

Colloidal semiconductor quantum dot (QDs) nanocrystals, synthesized via aqueous or hot injection routes, have drawn global attention within the past two decades. The unique properties of QDs, such as their broad absorption and emission spectra, excellent photostability, size-tunable photoluminescence (PL) spectra and multiplexing potentials have instigated their widespread applications in medical therapy, biological imaging, biomedical labelling, fluorescence sensing, solar cells and in opto-electronic device applications[1-9]. Some of the aims of fine-tuning their surface chemistry, structures and composition are to obtain a high PL quantum yield and improved photostability. Hence, it is vital to protect the QDs from their surrounding environment by passivating their surface against surface defects[10,11]. To achieve this, inorganic shell materials or organic ligands are generally employed as passivating materials. For organic ligands, they are generally employed to fine-tune the shape and size of the QDs, stabilize monomer concentrations during QD growth or nucleation and create new electronic states outside of the band gap by bonding to surface traps on the QD surface[12-14]. However, they do not provide total surface coverage of the QDs due to steric hindrance between adjacent ligands[15].

Conversely, more complete surface coverage of the QDs can be achieved with the use of inorganic shell materials, but the appropriate selection of a single shell material is a major challenge[12]. To date, the most widely used QDs manufactured by various synthetic strategies and the mixture of precursors are CdSe and CdTe, whilst the most commonly used type I shell materials (i.e., shell materials that exhibit a wider bandgap than the core) overcoated on their surfaces are CdS, ZnSe and ZnS. With reference to band energies and crystal lattice spacing, CdS and ZnSe have similar properties to those of CdSe and also share with it a common atom[16,17]**.** ZnS on the other hand, exhibits a much higher lattice mismatch compared to CdS and ZnSe and this enables its conduction and valence band energies to straddle those of CdSe and thus prevents the core excitons from reaching the QD surface, but it suffers from local strains and dislocations[18]**.** With respect to ease of growth, CdS and ZnSe can be more easily overcoated onto CdSe as compared to ZnS, due to their smaller lattice mismatch between the materials but they do not produce complete exciton confinement. Conversely, the excitons of ZnS can be more efficiently confined to the CdSe core due to its higher bandgap as compared to CdS and ZnSe. In order to circumvent this trade-off, several researchers have fabricated core/shell/shell QDs composed of CdSe/CdS/ZnS or CdSe/ZnSe/ZnS[19-22]. In general, the optical properties of shell materials deposited on non-alloyed core QDs have been well studied and reported in literature[23-25] but not much is known about the optical properties of shell materials deposited on alloyed core QDs[14,26].

To bridge this gap, we carried out an investigation to study the effects of deposition of multiple shell layers on alloyed CdSeTe core QDs. CdS, ZnSe and ZnS (the most

popular shell materials) were overcoated onto the alloyed ternary CdSeTe core in a one-pot synthetic approach. Conversion of the hydrophobic QDs nanocrystals to water-soluble nanocrystals was achieved using L-cysteine thiol ligand through a ligand exchange reaction. Ternary CdSeTe was chosen due to its superior electronic and optical properties generated from its strong nonlinear effect between the emission/absorption energies and composition[27]**.** To the best of our knowledge, the capping of L-cysteine onto the respective QDs via ligand exchange reaction and the synthesis and characterization of CdSeTe/CdS/ZnSe core/shell/shell (CSS) and CdSeTe/CdS/ZnSe/ZnS CSSS QDs are reported here for the first time. Our primary objective in this work is to investigate the effects of deposition of multiple shell layers on the alloyed core in order to draw conclusions on the optical properties of the respective QDs.

2. Experimental Section

2.1. Materials

Trioctylphosphine oxide (TOPO), cadmium oxide, sulphur, zinc oxide, 1-octadecene (ODE), tellurium powder, L-cysteine, zinc diethyldithiocarbamate (ZDC) and oleic acid (OLA) were purchased from Sigma Aldrich. Methanol, chloroform, acetone, selenium powder and potassium hydroxide were purchased from Merck. Solutions of the QDs were prepared with ultra pure water obtained from a Milli-Q Water System.

2.2. Characterization

UV-vis absorption spectra were recorded on a Cary Eclipse (Varian) spectrophotometer. Fluorescence emission spectra were recorded on a Horiba Scientific Fluoromax-4 spectrofluorometer. Determination of the PL quantum yield (Φ_F) of the QDs was achieved by comparing the integrated fluorescence intensities of the QDs (F) in Millipore water to that of Rhodamine 6G (F_{Std} ; $\Phi_{F(Std)}$ = 95%)[28] in ethanol whilst taking into consideration the refractive indices (n) of the solvents and absorbance of each QDs (A) and Rhodamine 6G (A_{Std}) at the excitation wavelength.

$$\Phi_F = \Phi_{F(Std)} \frac{F \,.\, A_{Std} \,.\, n^2}{F_{Std} \,.\, A \,.\, n_{Std}^2}$$

X-ray powder diffraction (XRD) patterns were analyzed using a PANalytical X'Pert Pro powder diffractometer in θ–θ configuration with an X'Celerator detector, variable divergence and receiving slits with Fe filtered Co-Kα radiation (λ=1.789Å). Transmission electron microscopy (TEM) images were obtained using a JEOL JEM 2100F operated at 200 kV. Fluorescence lifetime measurements were carried out using a time correlated single photon counting (TCSPC) setup (FluoTime 200, Picoquant GmbH). The excitation source was a diode laser (LDH-P-C-485 with 10 MHz repetition rate, 88 ps pulse width). Fluorescence was detected under the magic angle with a peltier cooled photomultiplier tube (PMT) (PMA-C 192-N-M, Picoquant) and integrated electronics (PicoHarp 300E, Picoquant GmbH). A monochromator with a spectral width of about 4 nm was used to select the required emission wavelength band. A scattering Ludox solution (DuPont) was used to measure the response function of the system and had a full width at half maximum (FWHM) of about 280 ps. To obtain good statistics, the ratio of stop to start pulses

was kept low (below 0.05). Measurement of the entire luminescence decay curve (range 0 to 100 ns) was at the maximum of the emission peak. Data analysis was done using the program Fluofit (Picoquant GmbH). Estimation of the decay error times was carried out using the support plane approach.

2.3. One-pot synthesis of the QDs

Alloyed CdSeTe, CdSeTe/CdS, CdSeTe/CdS/ZnSe and CdSeTe/CdS/ZnSe/ZnS QDs were synthesized via a modified method reported in literature for the synthesis of core/shell/shell QDs[14]. A hot injection method, employing successive injection of shell precursors in a one-pot step was adopted (Scheme 1, step 1). Typically, 1.3 g (10.1 mmol) of CdO was placed into a round-bottom three-necked flask containing a mixture of 30 mL OLA and 50 mL of ODE. The mixture was heated to 280 ^{o}C under reflux and degassed under Ar atmosphere with vigorous stirring. After the mixture produced a clear solution, a TOPSe solution containing Se (0.3 g, 3.8 mmol) dissolved in 5 mmol (1.93 g) TOPO and 5 mL of ODE was injected into the Cd-precursor solution. After 5 s of adding the TOPSe solution, the colour of the solution changed from colourless to deep-red which indicated the growth initiation of CdSe. Immediately after the solution changed from colourless to deep red, a solution of TOPTe containing Te (0.48 g, 3.8 mmol), dissolved in 5 mmol (1.93 g) TOPO and 25 mL of ODE was added. The temperature of the solution was still maintained at 270 ^{o}C to allow the nucleation of the as-prepared CdSeTe QDs. After 15 min, the temperature of the solution was lowered to 200 ^{o}C to prevent further growth of CdSeTe. Afterwards, a solution of 1.3 g (10.1 mmol) of CdO containing 5 mmol (1.93

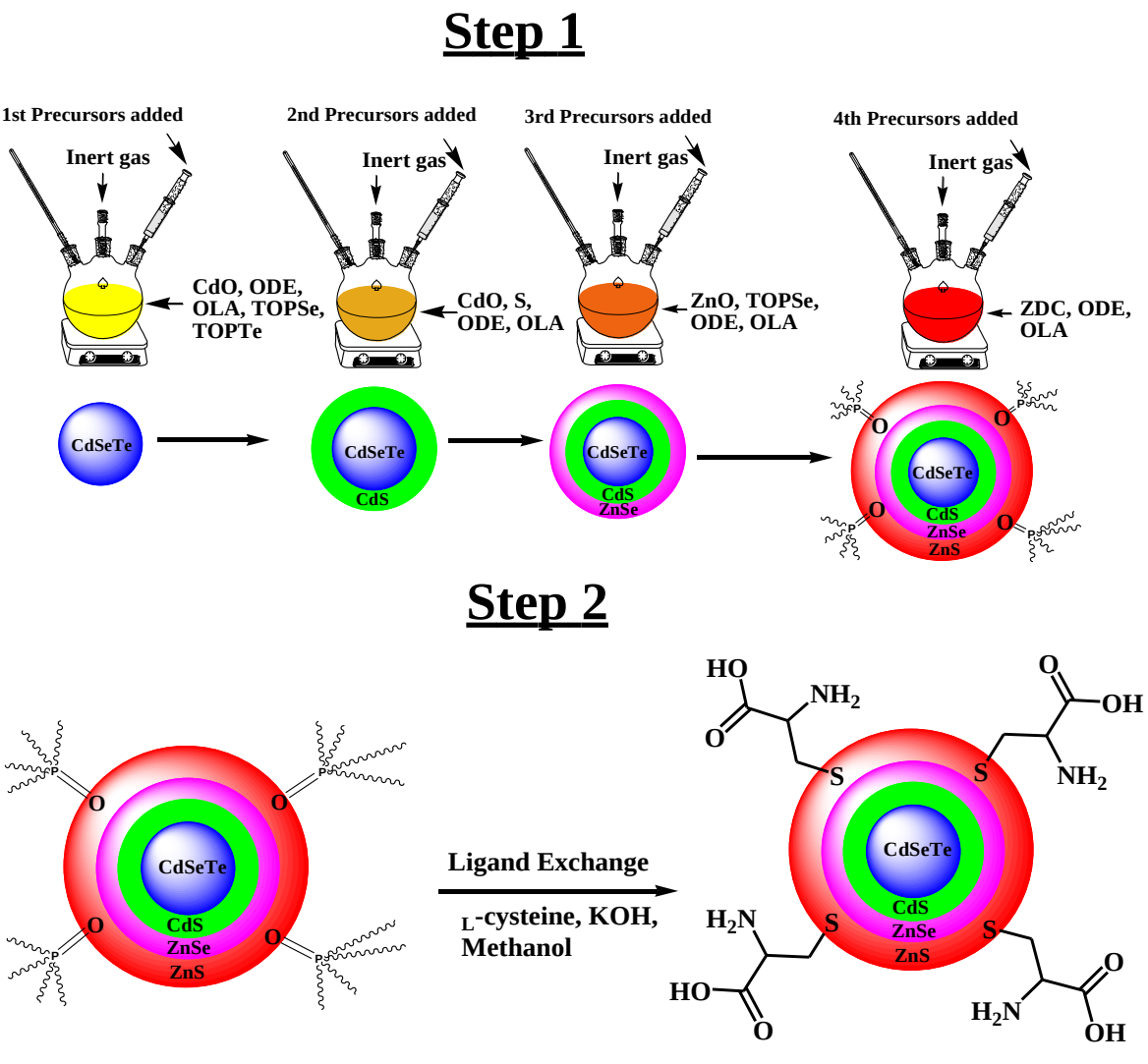

Scheme 1. Schematic representation of the synthesis and ligand exchange reaction of the QDs. CdSeTe/CdS/ZnSe/ZnS QDs is used as a representative QDs for ligand exchange reactions.

g) TOPO dissolved in 25 mL of ODE, and 0.16 g (5.0 mmol) of sulphur powder dissolved in 20 mL OLA and 30 mL ODE were added into the CdSeTe QDs growth solution to afford the overcoating of CdS shell on the CdSeTe core surface at a reduced temperature of 200 ^{o}C. Once the desired size of the CdSeTe/CdS core/shell QD was obtained, ZnO (0.407g, 5.0 mmol) dissolved in 20 mL OLA and 30 mL ODE and a TOPSe solution were injected into the CdSeTe/CdS QDs solution to afford the

growth of CdSeTe/CdS/ZnSe CSS QDs at a reduced temperature of 170 ^{o}C. Portion of zinc diethyldithio carbamate (2.2 mmol, 0.814 g) dissolved in 20 mL OLA and 30 mL ODE were alternately injected into the CdSeTe/CdS/ZnSe growth solution at a reduced temperature of 150 ^{o}C and at different time intervals to harvest each size of the CSSS QDs. This resulted in the overcoating of the ZnS QDs on the CdSeTe/CdS/ZnSe CSS surface. The QDs were purified with the addition of methanol followed by acetone.

2.4. Water-solubilization of the QDs

Firstly, a KOH-methanolic solution was prepared by dissolving 3 g of KOH in 40 mL of methanol after which 2 g of $_{L}$-cysteine was dissolved in it. Hydrophobic solutions of alloyed CdSeTe, CdSeTe/CdS, CdSeTe/CdS/ZnSe and CdSeTe/CdS/ZnSe/ZnS nanocrystals, dissolved in chloroform were added separately to the as-prepared KOH-methanolic solution containing $_{L}$-cysteine and 15 mL of Millipore water was additionally added (Scheme 1, step 2). Precipitation of the QDs nanocrystals occurred which allowed for the separation of the organic phase from the aqueous phase. The solutions were allowed to stir for about 15 min after which collection of the water-dispersible QDs nanocrystals was performed via repeated centrifugation with acetone. To completely remove unreacted organic layers, the QDs were subjected to further purification using a chloroform:water:acetone (1:1:3) mixture.

3. Results and discussion

3.1. Growth of the QDs

While most of the properties of alloyed QDs reported in literature have been induced from composition-tunable PL emission, in our work, a fixed concentration of the precursors was employed to fine-tune the comparison of the PL emission of the alloyed core to the final CSSS product. The objective of our work is to comparatively study the optical and structural properties of the as-prepared alloyed CdSeTe, CdSeTe/CdS, CdSeTe/CdS/ZnSe and CdSeTe/CdS/ZnSe/ZnS nanocrystals. In this work, the molar ratios employed were; Cd:Te:Se, 2.7:1.0:1.0 to fabricate the synthesis of the core CdSeTe, Cd:S, 2.0:1.0 for the overgrowth of the CdS shell and the same molar ratio was employed for the Zn cation and Se anion to overgrow the ZnSe shell layer. The fabrication of the mole ratios used in this work was adopted from our previous work in which a ligand exchange process was used to obtain water soluble 3-mercaptopropionic acid-capped CdSe/ZnS QDs with a quantum yield (Φ_F) value of 52 %[29]. From our initial assessment, we found out that based on our synthetic method, TOPSe was more reactive to CdO than TOPTe. Hence, TOPSe was deposited first into the reaction mixture before waiting for a period of few seconds to deposit the TOPTe precursor. We therefore suggest that an alloyed structure with CdSe-rich nuclei was formed. Generally, a one-pot approach was adopted for the fabrication of the QDs. We chose to overcoat CdS on the alloyed ternary CdSeTe core instead of the conventional CdSe core due to the non-blinking emission properties reported for the former. Also, CdSeTe alloys have been suggested to have a slight non-linear relationship between the composition and

energy band gap which thus relates to the phenomenon known as "optical bowing"[27]. However, it has been reported that the extent of optical bowing is more for homogenous alloys than for gradient alloys[27].

Alloyed CdSeTe was prepared in a non-coordinating solvent, ODE, at high temperature (280 ^{o}C) which involves a CdO-OLA complex with TOPSe and TOPTe as the Cd, Se and Te precursors. Experimental results showed that a strong coordinating capacity was achieved with the choice of the stabilizer OLA and surfactant TOPO, which subsequently led to an effective dispersion of alloyed CdSeTe core nanocrystal for subsequent shell growth. The reduced deposition temperature (200 ^{o}C), appropriate blends of reactivity of the precursors and the synergistic effect of the strong coordinating capacity of OLA and TOPO, ensured that heterogeneous nucleation of CdS prevailed at the surface interface of CdSeTe. This process prevented further growth of CdSeTe which is induced by atomic interdiffusion or Oswald ripening. Hence, the corresponding CdSeTe/CdS alloyed core/shell nanocrystal with the desired size and corresponding fluorescence emission wavelength was obtained.

Subsequently, a second ZnSe shell was epitaxially coated around the outer layer of the CdSeTe/CdS nanocrystal at a reduced temperature (170 ^{o}C) to form the CdSeTe/CdS/ZnSe core/shell/shell QDs. The choice of solvent system employed for overcoating CdS around CdSeTe to form the CdSeTe/CdS nanocrystal was also effective in overcoating the ZnSe shell around the CdSeTe/CdS template. To overcoat the third shell layer, ZDC was chosen as the single molecular precursor for ZnS because in the presence of appropriate capping agents, it decomposes to form

metal sulphide nanocrystals at an intermediate temperature and it has been reported to substantially preserve the fluorescence properties of the QDs especially when transferred from the organic phase to the aqueous phase[30].

3.2. Structural Properties

3.2.1. TEM analysis

Fig. 1A shows the TEM image of alloyed ternary CdSeTe core with an average particle size distribution of 2.6 nm and the TEM images of the corresponding CdSeTe/CdS, CdSeTe/CdS/ZnSe and CdSeTe/CdS/ZnSe/ZnS QDs which were derived from the initial CdSeTe core through the successive overgrowth of the respective CdS, ZnSe and ZnS shells are shown in Fig. 1B – 1E. The average particle size distribution of the dot-shaped CdSeTe/CdS core/shell nanocrystal increased to 3.2 nm whilst for the overgrowth of the ZnSe shell on the CdSeTe/CdS surface, the average size distribution increased to 3.4 nm. To epitaxially overgrow the ZnS shell layer around the CdSeTe/CdS/ZnSe nanocrystal, the amount of ZnS precursor was added at different time intervals based on the successive ion layer adsorption and reaction (SILAR) approach[31]. Fig. 1D and 1E shows an average particle size distribution of 3.8 nm and 4.1 nm for the TEM images of CdSeTe/CdS/ZnSe/ZnS QDs containing different volumes of added ZnS shell. The amount of added ZnS solution for CdSeTe/CdS/ZnSe/ZnS2 was twice that added for CdSeTe/CdS/ZnSe/ZnS1. We found out experimentally that the amount of injected shell precursors strongly influenced the fluorescence intensity and stability of the

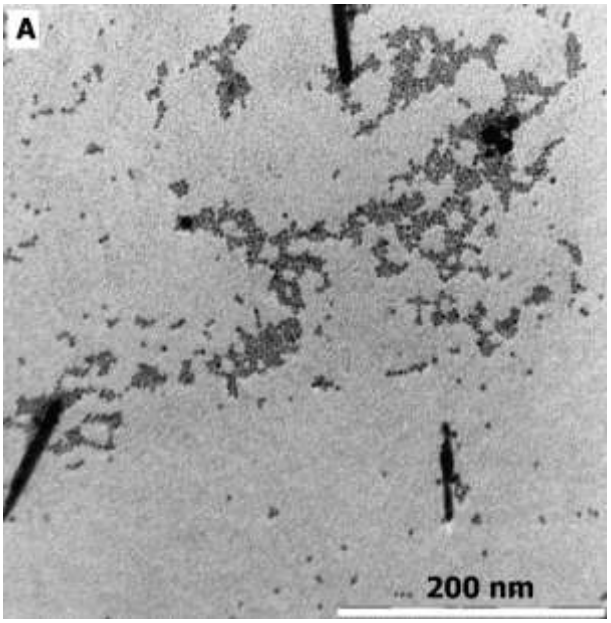
A
200 nm

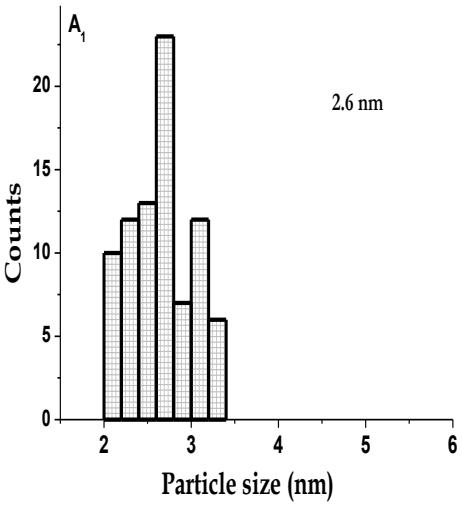
A1
2.6 nm
Counts
Particle size (nm)

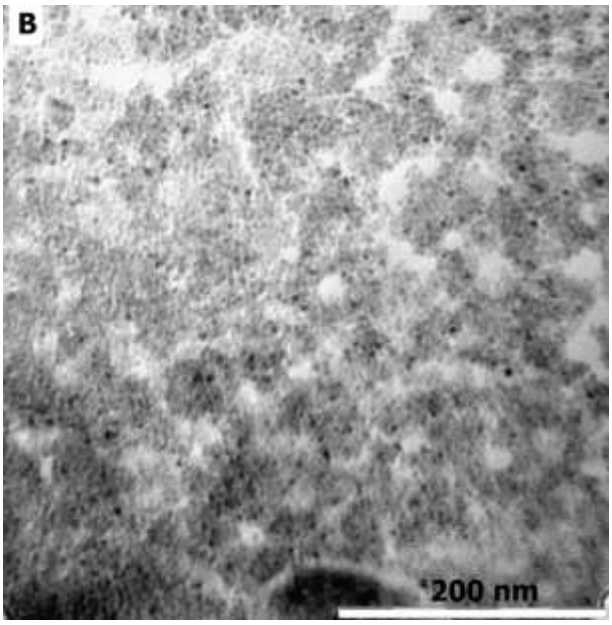
B
200 nm

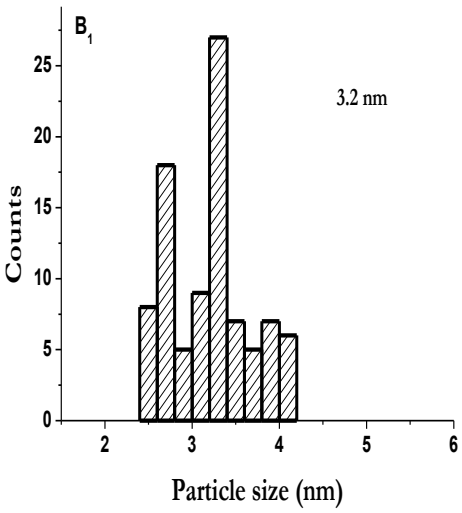
B1
3.2 nm
Counts
Particle size (nm)

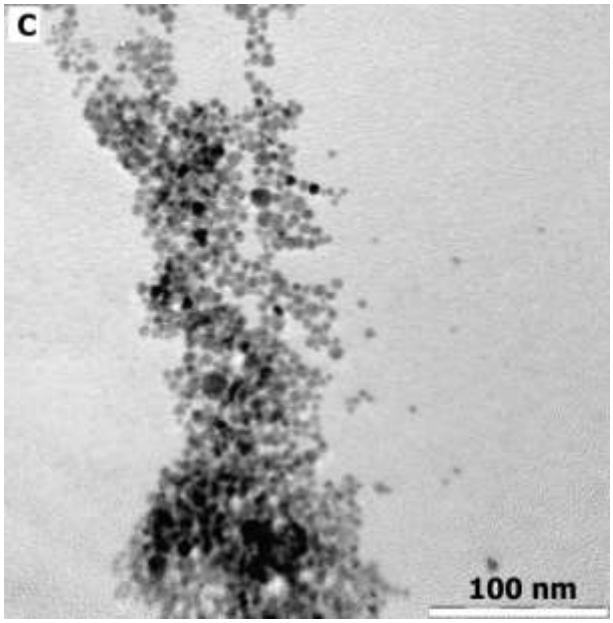
C
100 nm

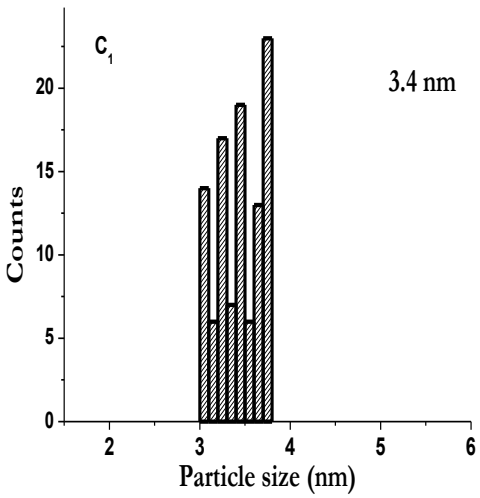
C1
3.4 nm
Counts
Particle size (nm)
0
5
10
15
20
2
3
4
5
6

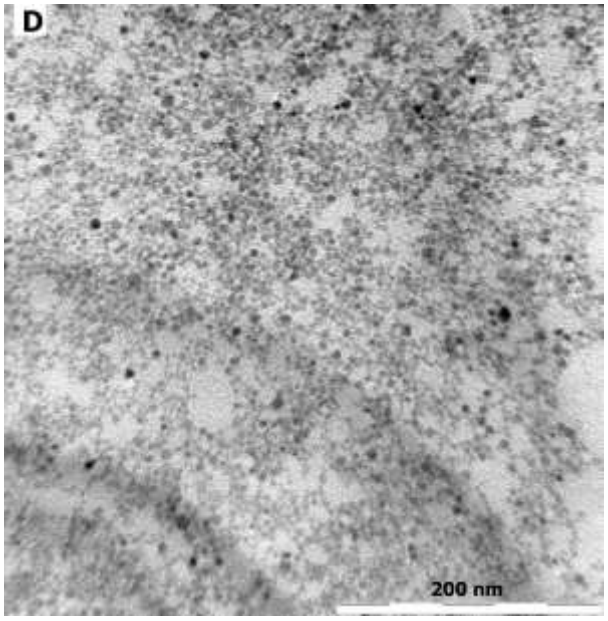
D
200 nm

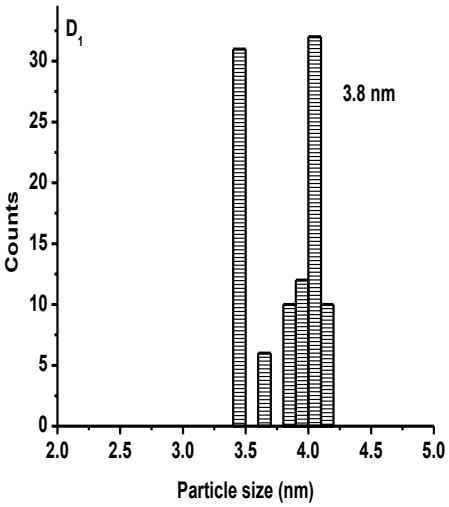
D1
3.8 nm
Counts
Particle size (nm)
0
5
10
15
20
25
30
2.0
2.5
3.0
3.5
4.0
4.5
5.0

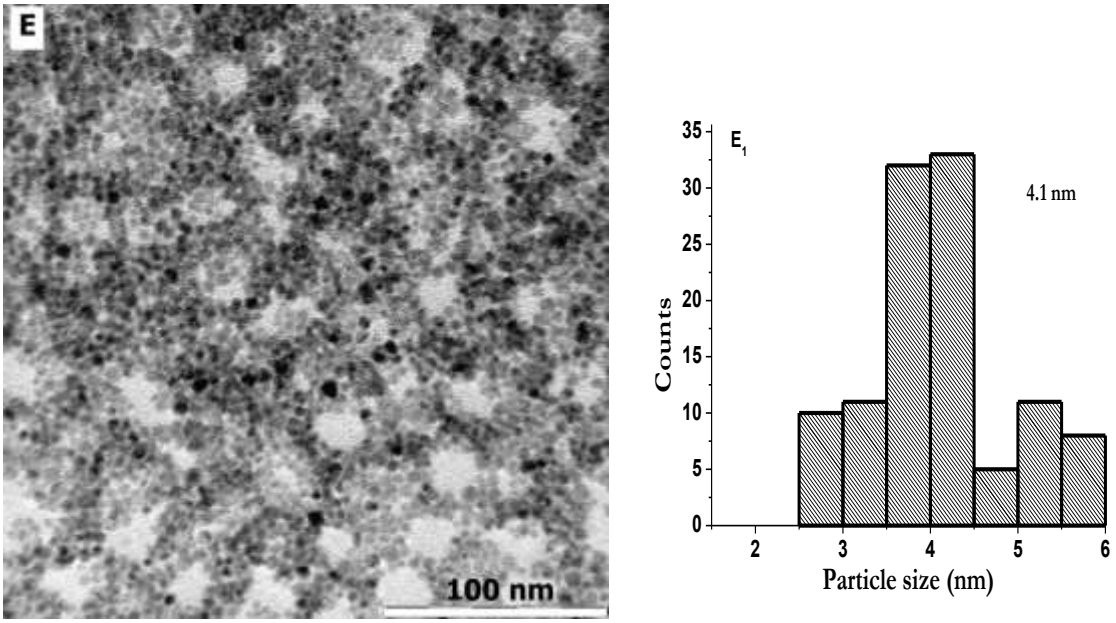

Figure 1. TEM images and the corresponding histograms of the particle size distribution of water-soluble alloyed (A) CdSeTe, (B) CdSeTe/CdS, (C) CdSeTe/CdS/ZnSe and (D) CdSeTe/CdS/ZnSe/ZnS corresponding to 50 mL of ZnS and (E) 100 mL of ZnS. The scale bars are not the same for all images.

QDs. Hence, an excess of shell precursors were added into the growth solution to form the corresponding QDs nanocrystals.

3.2.2. XRD Analysis

To understand the crystal nature of the alloyed ternary CdSeTe QDs, we have displayed the XRD pattern of L-cysteine-capped CdTe and CdSe QDs in comparison with CdSeTe QDs (Fig. 2). It is expected that if the diffraction pattern of CdSeTe QDs exhibits a superposition of pure CdTe and CdSe, then the prepared alloyed QDs are a mixture of binary CdTe and CdSe QDs rather than an alloyed composition. From the display of the diffraction patterns in Fig. 2, it can be seen that the diffraction

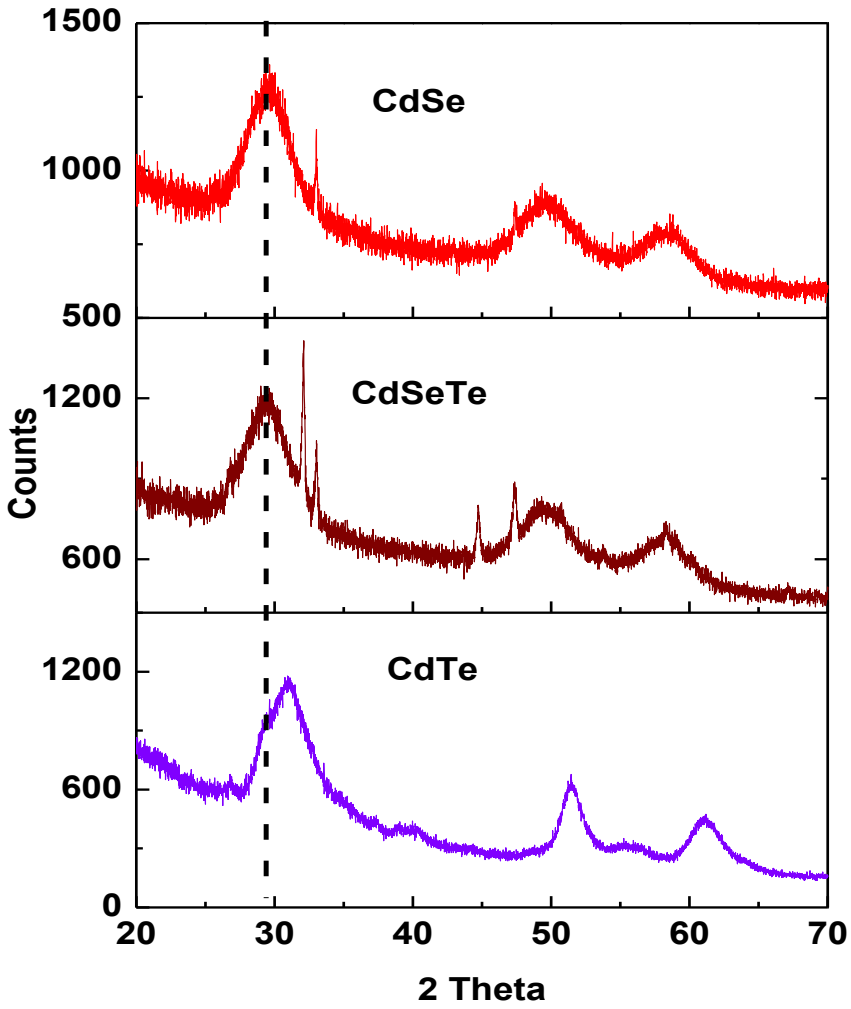

Figure 2. Powder XRD pattern for water-soluble L-cysteine-capped CdTe, CdSeTe and CdSe QDs.

peaks of CdTe are shifted to higher Bragg angle when compared to the diffraction peaks of CdSeTe while the diffraction pattern of CdSe and CdSeTe are nearly similar which confirms our earlier suggestion that the alloyed CdSeTe QD is composed of CdSe-rich nuclei.

Fig. 3 shows the powder XRD patterns of the alloyed CdSeTe core and the representative CdSeTe/CdS, CdSeTe/CdS/ZnSe and CdSeTe/CdS/ZnSe/ZnS nanocrystals. All the XRD patterns for the nanocrystals are similar and consist of the

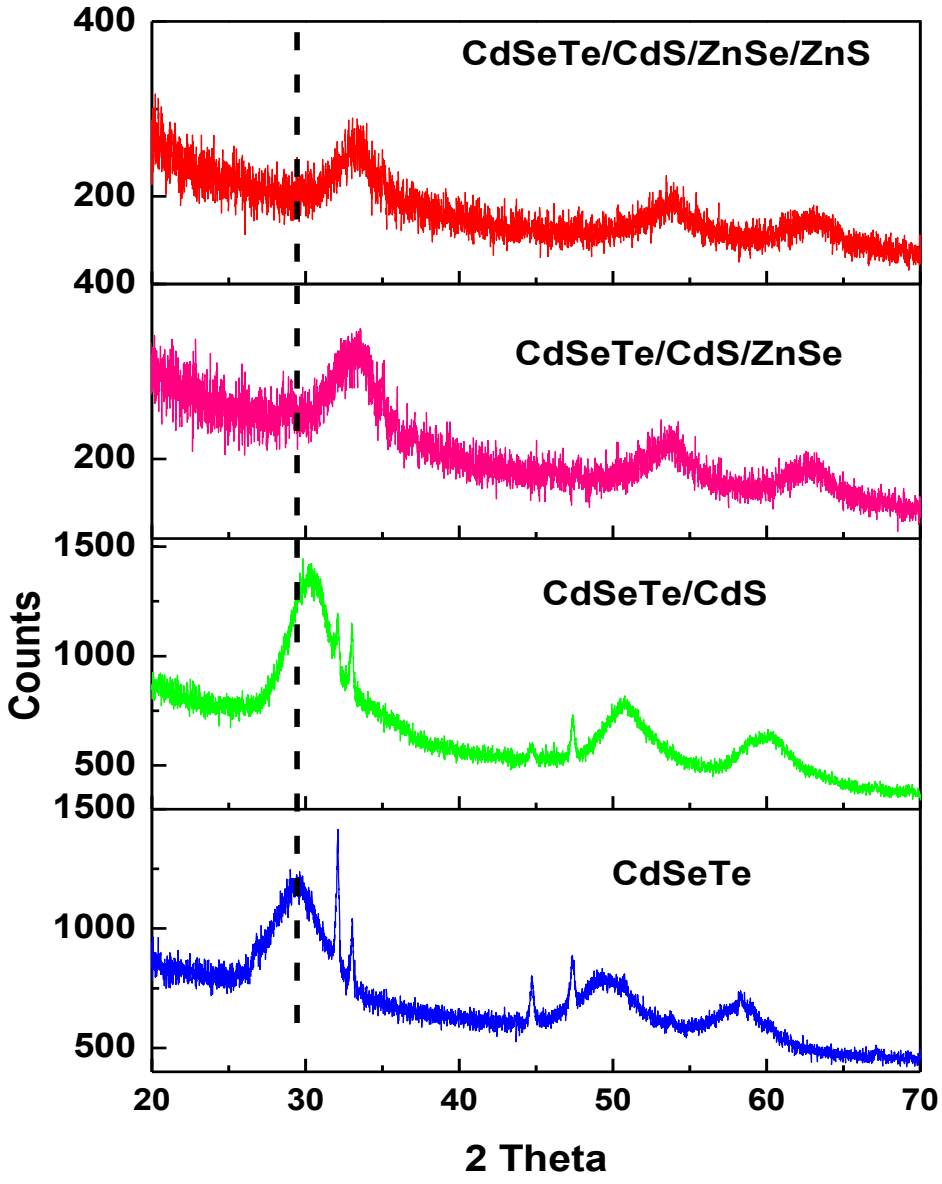

Figure 3. Powder XRD pattern for water-soluble alloyed L-cysteine-capped CdSeTe, CdSeTe/CdS, CdSeTe/CdS/ZnSe and CdSeTe/CdS/ZnSe/ZnS QDs.

characteristic peaks of cubic zinc blend crystal structure with planes at {111}, {220} and {311}. From the display of the diffraction patterns, we can exclude the possibility of a phase change. When the CdS shell is overgrown around the alloyed CdSeTe

core, it can be observed that the general pattern of the cubic lattice is consistent in the core/shell structure and there was a noticeable peak shift which confirms the formation of the CdSeTe/CdS core/shell QDs. Additionally, it could be seen that a narrowing of the diffraction peak was detected, which thus demonstrates an increase of the crystalline domain size. Further overgrowth of the ZnSe shell around the outer layer of CdSeTe/CdS revealed a well refined diffraction pattern with a further shift to higher Bragg angle. This clearly demonstrates the successive formation of the CdSeTe/CdS/ZnSe nanocrystal. However, upon coating of the ZnS shell layer on the CdSeTe/CdS/ZnSe surface, there was no noticeable peak shift. A lack of peak shift upon coating of ZnS shell layer on the CdTe/CdSe surface has also been reported by Zhang et al.[30]

3.3. Optical properties

3.3.1. UV/vis absorption and fluorescence measurements

The major challenge in producing water-soluble QDs via ligand exchange reaction is the dramatic loss in PL intensity upon conversion to the water phase[5]. The challenge of retaining the initial PL intensity of the QDs after ligand exchange has not been fully overcome to date. Hence, to avoid complete or significant loss of fluorescence after conversion to the water phase, effective control of the synthetic process is essential. In our work, the amount of shell precursors was carefully controlled during the QDs growth in order to produce highly fluorescent nanocrystals. Fig. 4 shows the evolution of the PL and absorption spectra of the respective CdSeTe, CdSeTe/CdS, CdSeTe/CdS/ZnSe and CdSeTe/CdS/ZnSe/ZnS nanocrystals. The

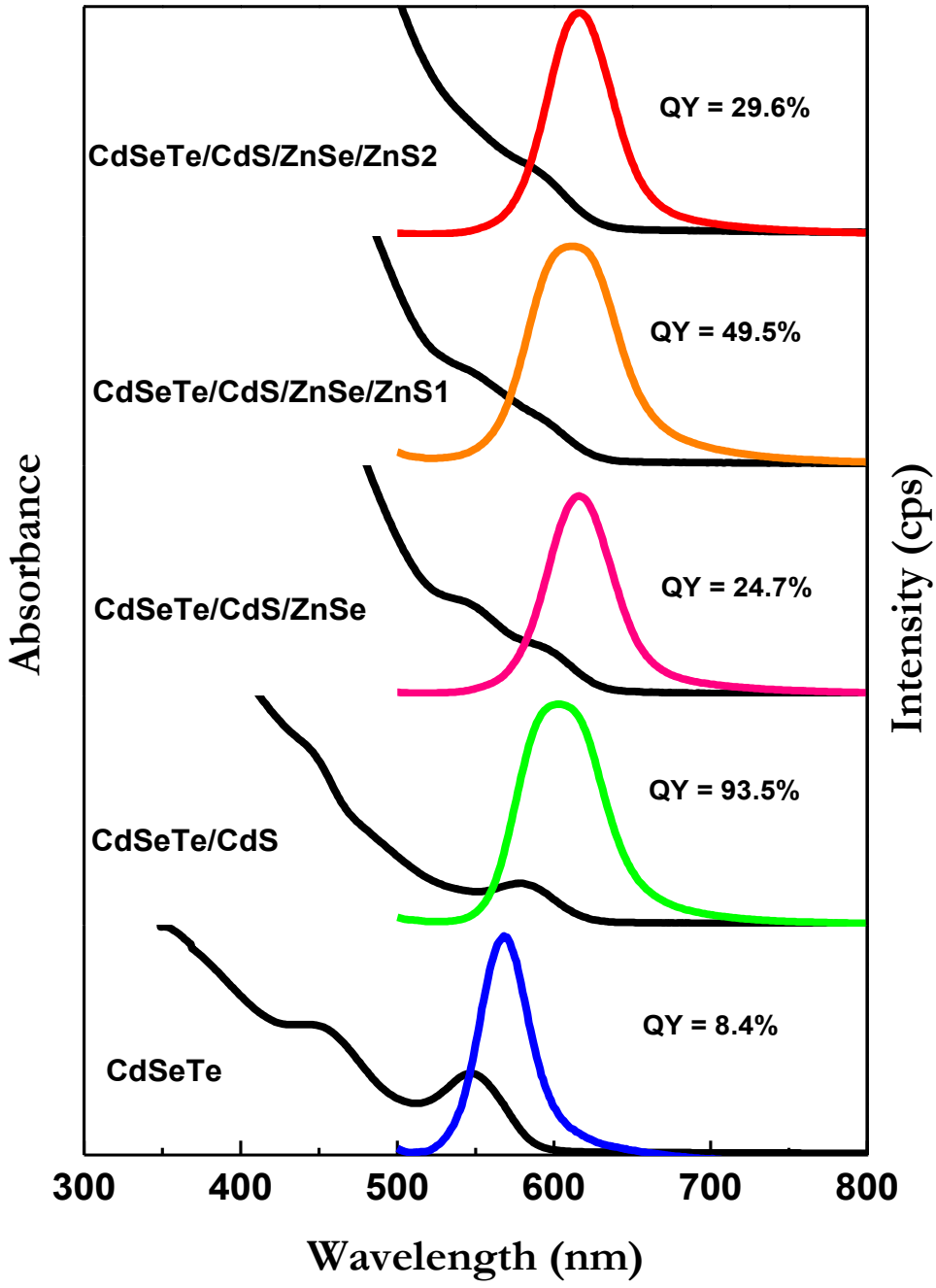

Figure 4. UV-vis absorption and fluorescence emission spectra of the water-soluble alloyed CdSeTe, CdSeTe/CdS, CdSeTe/CdS/ZnSe, CdSeTe/CdS/ZnSe/ZnS1 (50 mL of ZnS) and CdSeTe/CdS/ZnSe/ZnS2 (100 mL of ZnS) QDs measured in Millipore water. λ_{exc} = 470 nm.

PL emission wavelength of the corresponding QDs measured in Millipore water are CdSeTe (λ_{em} = 569 nm), CdSeTe/CdS (λ_{em} = 604 nm), CdSeTe/CdS/ZnSe (λ_{em} = 616 nm), CdSeTe/CdS/ZnSe/ZnS1 (λ_{em} = 612 nm) and CdSeTe/CdS/ZnSe/ZnS2 (λ_{em} = 616 nm).

The nature of the barriers with reference to the electronic environment for the core and shell in the core-shell interface is the criterion which determines the red-shift between the core and core-shell QDs. In addition, the parameter which is known to instigate a strain-induced shift between the core and shell in the absorption spectrum of the core-shell nanocrystals is called the lattice mismatch[18]. Typically for CdSe/CdS core-shell QDs, a significant red-shift in the absorption spectrum relative to the core is not expected due to the small lattice mismatch (3.7 %) between the CdSe core and CdS shell[16]. As shown in Fig. 4, when comparing the absorption spectra of the QDs, we noticed the absorption spectra of CdSeTe and CdSeTe/CdS QDs displayed a clear excitonic peak which showed slight broadening as the core-shell structure was formed. The formation of CdSeTe/CdS QDs induced a significant red-shift of 35 nm in the PL emission spectrum after the deposition of the CdS shell. In our work, we observed that the extent of the red-shift was not influenced by the added amount of Cd and S precursors. The SILAR approach also was not successful to induce further red-shifting of the PL emission of the core/shell QDs even after several hours of the reaction process. With reference to the photophysical properties of the QDs, CdSeTe produced a PL quantum yield (QY) value of 8.4% which increased dramatically to a value of 93.5 % when the CdS shell was passivated on the CdSeTe surface. The increase in the QY value suggests a well

passivated surface, low defect concentrations and elimination of the nonradiative recombination rates of the high quality CdSeTe/CdS core/shell QDs manufactured in this work. The low, if not negligible, surface defect concentrations may be due to a combination of a well controlled synthetic process with reference to a slow epitaxial growth and an effective surface reconstruction and relaxation[30].

Judging by the similarities between the spectral shapes of the ground-state absorption peak for CdSeTe/CdS core/shell and core CdSeTe QDs, our as-synthesized L-cysteine-capped CdSeTe/CdS QDs could be considered to exhibit a quasi-type-II core/shell. For quasi-type-II core/shell QDs, the core serves as a platform for the absorption at the band gap. This occurs because the spatially indirect core/shell transition has a lower transition matrix element than the spatially direct transitions in the core. This is in contrast to type-II QDs with a larger band offset in which the absorption spectrum of the QDs is evidently broadened with a long red tail and the spatially indirect transitions prevails for QDs with larger shell thickness[18,32].

An attempt was further made in our work to overcoat ZnSe around the CdSeTe/CdS surface in order to study the resultant photophysical properties of these QDs in comparison to the CdSeTe/CdS core/shell QDs. A noticeable broadening of the absorption peak and a PL emission red-shift of 12 nm was observed for the CdSeTe/CdS/ZnSe QDs when compared to that of the core/shell nanocrystal. Also, the QY yield decreased markedly to 24.7 %. The sudden decrease in the QY value upon formation of the CdSeTe/CdS/ZnSe QDs prompted us to epitaxially overgrow an additional ZnS layer around the CdSeTe/CdS/ZnSe surface with the hope of

improving the QY value of the QDs. We adopted the SILAR approach for the epitaxial overgrowth of ZnS shell in which the ZnS precursor was added slowly at different time intervals. We however noticed that a small amount of the ZnS material did not induce any changes in the PL intensity of the QDs, hence a large excess of the ZnS shell materials was added at different time intervals into the growth solution. As shown in Fig. 4, addition of 50 mL of ZnS shell resulted in a dramatic increase of the QY value to 49.5 % and this also resulted in a significant increase in the PL intensity of the resultant CdSeTe/CdS/ZnSe/ZnS1 nanocrystal as shown in Fig. 5. The QY increase was accompanied by a slight blue shift (4 nm) in PL emission as shown in Fig. 3. Such a blue shift upon deposition of the ZnS layer has been reported in literature[33,34]**.** The phenomenon may be attributed to the fact that the Zn atoms diffuse at a fast rate into the ZnSe shell layer and thus provided effective confinement and elevated the band-offset of the shell material[33]**.** However, upon addition of another 50 mL of ZnS shell to the CdSeTe/CdS/ZnSe/ZnS1 nanocrystal, the QY value of the resultant QD decreased to a value of 29.6 % and this was also reflected by a decrease in the PL intensity of the resultant CdSeTe/CdS/ZnSe/ZnS2 when compared to the PL intensity of CdSeTe/CdS/ZnSe/ZnS1 (Fig. 5). In addition, the PL emission of CdSeTe/CdS/ZnSe/ZnS2 was red-shifted by 4 nm to the same PL emission of CdSeTe/CdS/ZnSe. Further deposition of an additional volume of ZnS was unsuccessful due to significant quenching of the fluorescence of the QDs. The decrease in the QY observed for both CdSeTe/CdS/ZnSe and CdSeTe/CdS/ZnSe/ZnS2 QDs could be due to a number of mechanisms such as: (i) the deposition of the shell layer with respect to its thickness could create strain

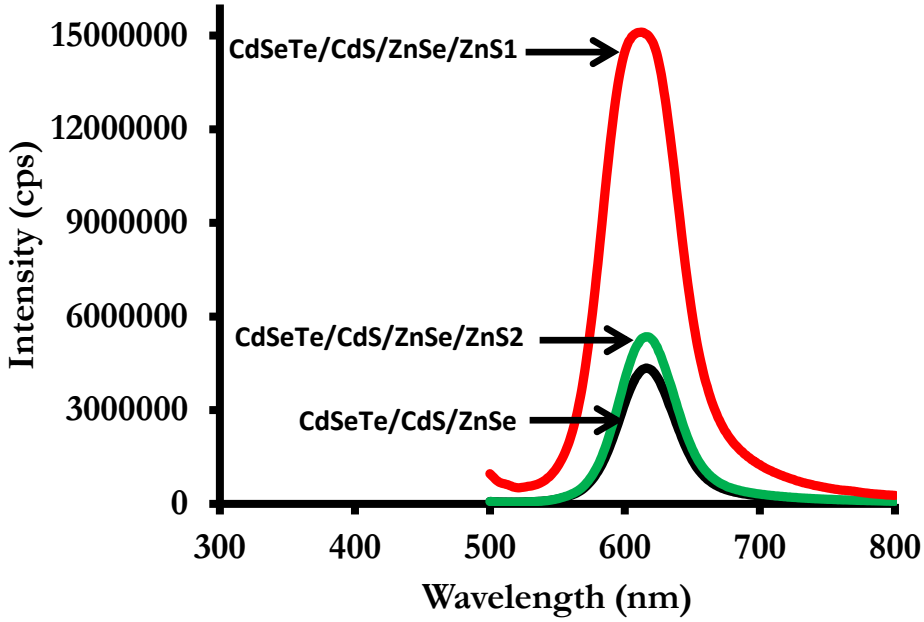

Figure 5. Variation in the PL intensity of water-soluble CdSeTe/CdS/ZnSe, CdSeTe/CdS/ZnSe/ZnS1 (50 mL ZnS) and CdSeTe/CdS/ZnSe/ZnS2 (100 mL ZnS) QDs. λ_{exc} = 470 nm.

through the creation of dislocations[35] and (ii) ZnSe and 100 mL of ZnS solution probably did not produce a strong quantum dot confinement effect[36]. Hence we can conclude that the CdSeTe/CdS QDs formed are of good quality due to their high PL QY, while the additional passivation of shell layers on their surface is not necessary since the PL QY of the respective CSS and CSSS QDs declined in comparison to the core/shell QDs. This further implies that CS QDs will be useful in a wide array of biological and chemical applications. Reported PL QY values of other types of CdSeTe-based CS QDs are: CdSeTe/CdZnS (QY = 50%)[37,38], CdSeTe/CdZnS (QY = 65%)[39] and CdSeTe/ZnS (QY = 70%)[40], respectively. Hence, the high PL QY value found for our CS QDs (QY = 94%) demonstrates their superior optical properties.

In Table 1, a summary of the optical properties of the QDs are given and it can be seen that the full width at half maximum (FWHM) of the QDs ranged from 43 to 63 nm.

Table 1. Summary of the photophysical properties of CdSeTe, CdSeTe/CdS, CdSeTe/CdS/ZnSe, CdSeTe/CdS/ZnSe/ZnS1 and CdSeTe/CdS/ZnSe/ZnS2 QDs.

QDs	τ_1 (ns)[a]	τ_2 (ns)[a]	τ_3 (ns)[a]	Mean lifetime (ns)	Average size (nm)	QY (%)	FWHM (nm)
CdSeTe	35.0(0.56)	8.4(0.35)	2.1(0.09)	15.2	2.6	8.4	43
CdSeTe/CdS	18.0(0.36)	4.0(0.39)	0.9(0.25)	7.6	3.2	93.5	63
CdSeTe/CdS/ZnSe	30.3(0.64)	7.8(0.31)	1.9(0.05)	13.3	3.4	24.7	55
CdSeTe/CdS/ZnSe/ZnS1	12.4(0.22)	2.7(0.46)	0.6(0.32)	5.2	3.8	49.5	63
CdSeTe/CdS/ZnSe/ZnS2	14.8(0.25)	3.0(0.46)	0.7(0.29)	6.2	4.1	29.6	54

[a]Relative abundance in brackets

3.3.2. Stability of the QDs

For biological and chemical applications requiring prolonged release of photons, it is important that the fluorescence intensity of the QDs remains constant irrespective of its surrounding environment. Hence, the fluorescence stability of the QDs were investigated by retaining the QDs in an aqueous solution for 7 days and measuring their fluorescence emission thereafter. If the QDs are unstable, aggregation will occur and this will be accompanied by precipitation of the QDs from solution with an apparent quenching of their fluorescence or tailing in their emission spectra. Fig. 6 shows the fluorescence emission spectra of the QDs measured after seven days in solution. The QDs were exposed to ambient light when in solution and as shown for

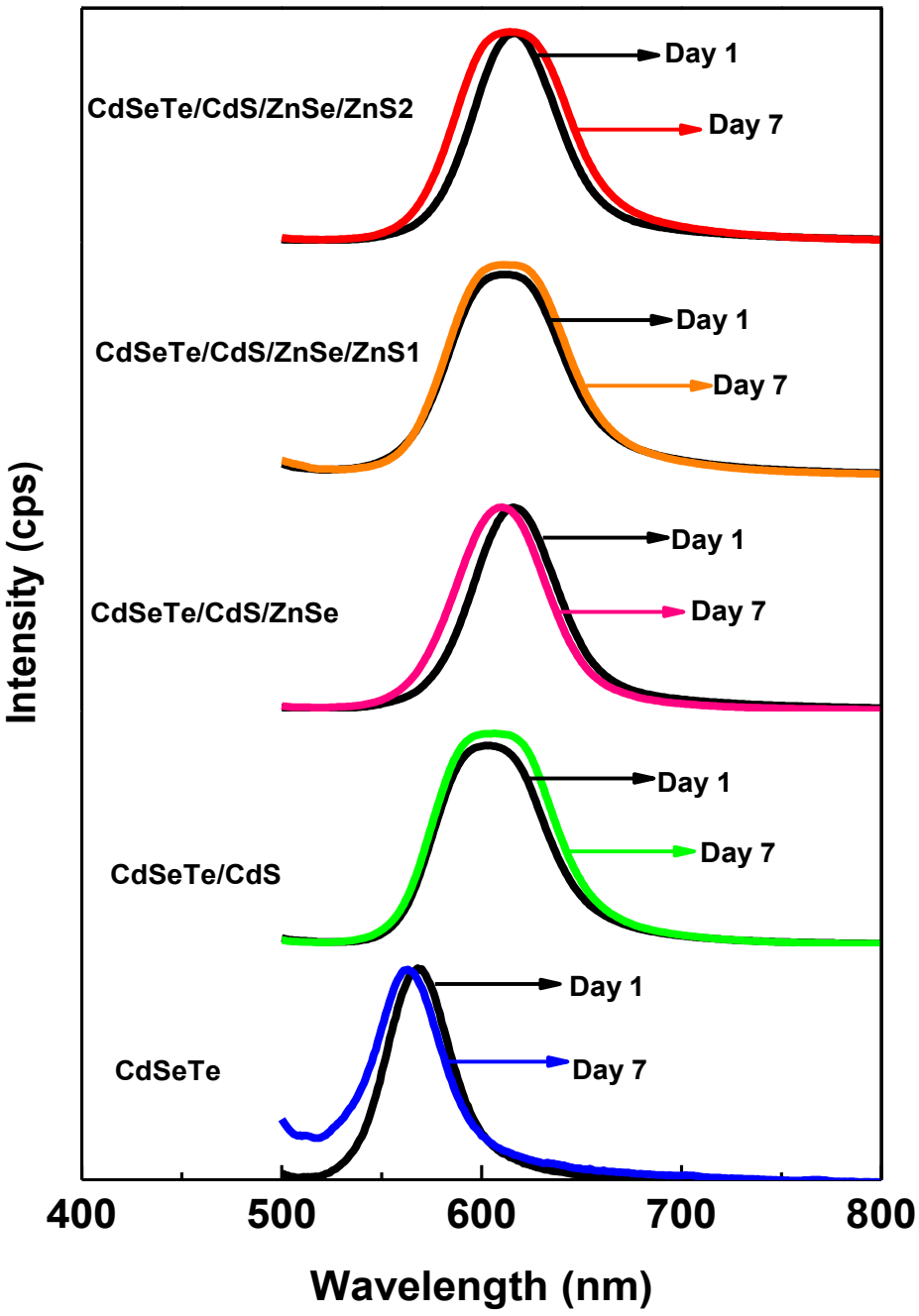

Figure 6. Fluorescence stability of the QDs measured before and after 7 days in aqueous solution. λ_{exc} = 470 nm.

CdSeTe core QDs, a degree of tailing of the emission peak can be observed after 7 days of measurement. Although, no quenching of the fluorescence emission was

apparent, the tailing in the emission peak indicates that the core QDs were relatively unstable. For CdSeTe/CdS QDs, there was no tailing or quenching of the fluorescence after 7 days of measurement which clearly demonstrates the strong passivation of the CdS shell and protection of the core QDs from photo-initiated degradation. The strong stability of CdSeTe/CdS/ZnSe and CdSeTe/CdS/ZnSe/ZnS QDs after 7 days of measurement was also confirmed as shown in Fig. 6. Even though CdSeTe/CdS/ZnSe and CdSeTe/CdS/ZnSe/ZnS QDs both exhibited good PL stability, which implies that they may be useful in applications requiring prolonged stability of the QD fluorescence, such as in biological imaging, their inferior PL QY in comparison to CdSeTe/CdS QDs indicates that they will exhibit lower sensitivity than the later in applications such as sensing/biosensing of analytes.

3.3.3. Time-resolved PL measurements

Time-resolved PL lifetime measurements were carried out on all the QDs to investigate the variation in the QY of the QDs on deposition of the shell materials. As shown in Fig. 7 and Table 1, the PL decay curves of the QDs were successfully fitted to triexponential PL lifetimes. For the core, CS, CSS and CSSS QDs, there were significant differences in their PL lifetime values which corroborated well with the measured variation in their QY values. From our work, it was observed that the QY value of CdSeTe/CdS core/shell QDs increased to 93.5 % on deposition of the CdS shell on the core CdSeTe surface. Assessing the mean PL lifetime values of CdSeTe core displayed in Table 1, it is clearly evident that a slow decay (higher PL lifetime)

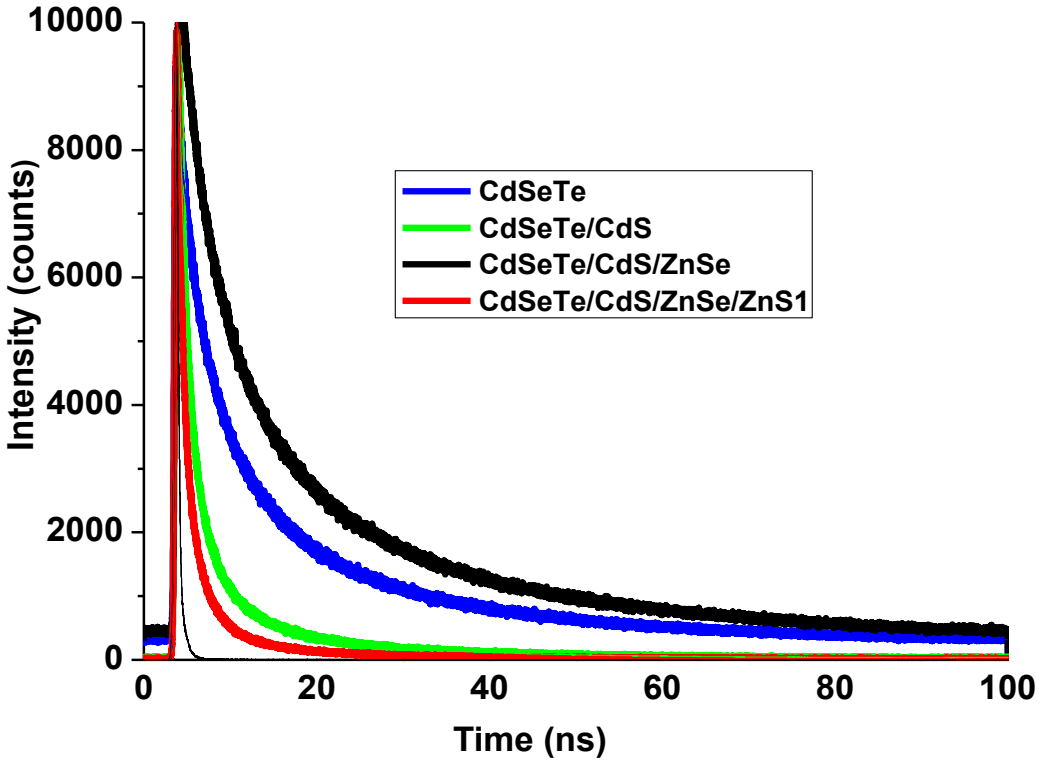

Figure 7. Time-resolved PL decay curves of CdSeTe, CdSeTe/CdS, CdSeTe/CdS/ZnSe, CdSeTe/CdS/ZnSe/ZnS1 nanocrystals measured in Millipore water.

was observed relative to the fast exciton decay (lower PL lifetime) for CdSeTe/CdS QDs. This suggests that the decreased PL lifetime and improved QY value of the resultant CdSeTe/CdS QDs was due to the elimination of the non-radiative recombination pathways and removal of surface defects in the core/shell system. Deposition of the ZnSe shell layer triggered a slow decay function as shown in Table 1 and this was also reflected in the significant decrease in the QY value of the resultant CdSeTe/CdS/ZnSe QDs. Upon addition of a 50 mL of ZnS shell to the CdSeTe/CdS/ZnSe system, the PL lifetime decayed on a fast scale with a dramatic increase in the QY value but the addition of another 50 mL of ZnS shell induced a

slight increase in the PL lifetime accompanied by a decrease in the QY of the QDs. Considering the complimentary data obtained from the QY value and PL lifetime measurements of the QDs, we suggest that the presence of the shell materials induced a radiative and nonradiative recombination processes depending on the surface state of the QDs.

4. Conclusions

The influence of shell deposition on the optical properties of alloyed CdSeTe core QDs has been investigated. CdSeTe/CdS exhibited a high QY value of 93.5 % which was a dramatic increase from 8.4 % value for the CdSeTe core. Formation of CdSeTe/CdS/ZnSe decreased the QY value to 24.7 % while the adoption of the SILAR approach improved the QY value of the resultant CdSeTe/CdS/ZnSe/ZnS QDs to 49.5 %. Time-resolved PL measurements provided useful insights into the variation in the photophysical properties of the QDs with respect to nonradiation and radiation recombination processes.

Acknowledgement

O. Adegoke thanks the University of Pretoria for a postdoctoral fellowship. This work is based on the research supported in part by the National Research Foundation of South Africa, Grant Number: 92584 (P. Forbes). Wirsam Scientific, South Africa is thanked for their support of this research. We thank the Electron Microscopy Unit, University of Pretoria (UP), for assistance with the TEM measurements and Wiebke Grote of UP for the XRD measurements.

References

1. Callan J, De Silva AP, Mulrooney RC, McCaughan B. Luminescent sensing with quantum dots. J Inclusion Phenom Macrocyclic Chem 2007;58:257-62.
2. Somers RC, Bawendi MG, Nocera DG. CdSe nanocrystal based chem-/bio- sensors. Chem Soc Rev 2007;36:579-91.
3. Bruchez M, Moronne M, Gin P, Weiss S, Alivisatos AP. Semiconductor Nanocrystals as Fluorescent Biological Labels. Science 1998;281:2013-16.
4. Yu WW, Chang E, Falkner JC, Zhang JY, Al-Somali AM, Sayes CM, Johns J, Drezek R, Colvin VL. Forming Biocompatible and Non-Aggregated Nanocrystals in Water Using Amphiphilic Polymers. J Am Chem Soc 2007;129:2871-79.
5. Yu WW. Semiconductor Quantum Dots: Synthesis and Water- Solubilization for Biomedical Applications. Expert Opin Biol Ther 2008;8:1571-81.
6. Tessler N, Medvedev V, Kazes M, Kan S, Banin U. Efficient Near-Infrared Polymer Nanocrystal Light-Emitting Diodes. Science 2002;295:1506-08.
7. Zhang Y, Xie C, Su HP, Liu J, Pickering S, Wang YQ, Yu WW, Wang JK, Wang YD, Hahm J, Dellas N, Mohney SE, Xu J. Employing Heavy Metal-Free Colloidal Quantum Dots in Solution-Processed White Light-Emitting Diodes. Nano Lett 2011;11:329-32.
8. Huynh WU, Dittmer JJ, Alivisatos AP. Hybrid Nanorod-Polymer Solar Cells Science 2002:295:2425-27.
9. Winiarz JG, Zhang L, Lal M, Friend CS, Prasad PN. Observation of the Photorefractive Effect in a Hybrid Organic- Inorganic Nanocomposite. J Am Chem Soc 1999;121:5287-95.
10. Gul S, Cooper JK, Corrado C, Vollbrecht B, Bridges F, Guo J, Zhang JZ. Synthesis, optical and structural properties, and charge carrier dynamics of Cu-doped ZnSe nanocrystals. J Phys Chem C 2011;115:20864-75.

11. Fitzmorris RC, Cooper JK, Edberg J, Gul S, Guo J, Zhang JZ. Synthesis and Structural, Optical, and Dynamic Properties of Core/Shell/Shell CdSe/ZnSe/ZnS Quantum Dots. J Phys Chem C 2012;116:25065-73.
12. Mokari T, Banin U. Synthesis and Properties of CdSe/ZnS Core/Shell Nanorods. Chem Mater 2003;15:3955-60.
13. Margaret A, Hines PG. Synthesis and characterization of strongly luminescing ZnS-capped CdSe nanocrystals. J Phys Chem 1996;100:468-71.
14. Fitzmorris BC, Pu Y-C, Cooper JK, Lin Y-F, Hsu Y-J, Li Y, Zhang JZ. Optical Properties and Exciton Dynamics of Alloyed Core/Shell/Shell $Cd_{1-x}Zn_xSe$/ZnSe/ZnS Quantum Dots. Appl Mater Interface 2013;5:2893-900.
15. Lees EE, Gunzburg MJ, Nguyen TL, Howlett GJ, Rothacker J, Nice EC, Clayton AH, Mulvaney P. Experimental determination of quantum dot size distributions, ligand packing densities, and bioconjugation using analytical ultracentrifugation. Nano Lett 2008;8:2883-990.
16. Peng X, Schlamp MC, Kadavanich AV, Alivisatos A. Epitaxial growth of highly luminescent CdSe/CdS core/shell nanocrystals with photostability and electronic accessibility. J Am Chem Soc 1997;119:7019-29.
17. Nice EC, Clayton AHA, Mulvaney P. Experimental determination of quantum dot size distributions, ligand packing densities, and bioconjugation using analytical ultracentrifugation. Nano Lett 2008;8:2883-90.
18. Dabbousi BO, Rodriguez-Viejo J, Mikulec FV, Heine JR, Mattoussi H, Ober R, Jensen KF, Bawendi MG. (CdSe)ZnS core−shell quantum dots: synthesis and characterization of a size series of highly luminescent nanocrystallites. J Phys Chem B 1997;101:9463-75.
19. Talapin DV, Mekis I, Goetzinger S, Kornowski A, Benson O, Weller H. CdSe/CdS/ZnS and CdSe/ZnSe/ZnS core-shell-shell nanocrystals. J Phys Chem B 2004;108:18826-31.

20. Jones M, Lo SS, Scholes GD. Quantitative modeling of the role of surface traps in CdSe/CdS/ZnS nanocrystal photoluminescence decay dynamics. Proc Natl Acad Sci USA 2009;106:3011-16.
21. Deka S, Quarta A, Lupo MG, Falqui A, Boninelli S, Giannini C, Morello G, De Giorgi M, Lanzani G, Spinella C. CdSe/CdS/ZnS double shell nanorods with high photoluminescence efficiency and their exploitation as biolabeling probes. J Am Chem Soc 2009;131:2948-58.
22. McBride J, Treadway J, Feldman L, Pennycook SJ, Rosenthal SJ. Structural basis for near unity quantum yield core/ shell nanostructures. Nano Lett 2006;6:1496-1501.
23. Wei F, Lu X, Wu Y, Cai Z, Liu L, Zhuo P, Hu Q. Synthesis of highly luminescent CdTe/CdS/ZnS quantum dots by a one-pot capping method. Chem Eng J 2013;226:416-22.
24. He H, Sun X, Wang X, Xu H, Synthesis of highly luminescent and biocompatible CdTe/CdS/ZnS quantum dots using microwave irradiation: a comparative study of different ligands. Luminescence 2014;29:837-45.
25. Taniguchi S, Green M, Rizvi SB, Seifalian A. The one-pot synthesis of core/shell/shell CdTe/CdSe/ZnSe quantum dots in aqueous media for in vivo deep tissue imaging. J Mater Chem 2011;21:2877-82.
26. Li L, Chen Y, Li Q, Li J, Shen Y, Xu M, Fei R, Yang G, Zhang K, Zhang J-R, Zhu J-J. Electrochemiluminescence energy transfer-promoted ultrasensitive immunoassay using near-infrared-emitting CdSeTe/CdS/ZnS quantum dots and gold nanorods. Scientific Reports 2013;3:1528.
27. Bailey RE, Nie SM. Alloyed semiconductor quantum dots: Tuning the optical properties without changing the particle size. J Am Chem Soc 2003;125:7100-06.

28. Magde D, Wong R, Seybold PG. Fluorescence quantum yields and their relation to lifetimes of rhodamine 6G and fluorescein in nine solvents: Improved absolute standards for quantum yields. Photochem Photobiol 2002;75:327-34.
29. Adegoke O, Nyokong T. Conjugation of mono-substituted phthalocyanine derivatives to CdSe@ZnS quantum dots and their applications as fluorescent-based sensors. Synthetic Met 2014;188:35-45.
30. Zhang W, Chen G, Wang J, Ye B-C, Zhong X. Design and synthesis of highly luminescent near-infrared-emitting water-soluble CdTe/CdSe/ZnS core/shell/shell quantum dots. Inorg Chem 2009;48:9723-31.
31. Li J, Wang Y, Guo W, Keay JC, Mishima TD, Johnson MB, Peng X. Large-scale synthesis of nearly monodisperse CdSe/CdS core/shell nanocrystals using air-stable reagents via successive ion layer adsorption and reaction. J Am Chem Soc 2003;125:12567-75.
32. Sugunan A, Zhao Y, Mitra S, Dong L, Li S, Popov S, Marcinkevicious S, Toprak MS, Muhammed M. Synthesis of tetrahedral quasi-type-II CdSe–CdS core–shell quantum dots. Nanotechnology 2011;22:425202.
33. Xie R, Kolb U, Li J, Basché T, Mews A. Synthesis and characterization of highly luminescent CdSe-Core CdS/$Zn_{0.5}Cd_{0.5}S$/ZnS multishell nanocrystals. J Am Chem Soc 2005;127:7480-88.
34. Shen H, Wang S, Wang H, Niu J, Qian L, Yang Y, Titov A, Hyvonen J, Zheng Y, Li LS. Highly efficient blue−green quantum dot light-emitting diodes using stable low-cadmium quaternary-alloy ZnCdSSe/ZnS core/ shell nanocrystals. Appl Mater Interfaces 2013;5:4260-65.
35. Hines MA, Guyot-Sionnest P. Synthesis and characterization of strongly luminescing ZnS-capped CdSe nanocrystals. J Phys Chem 1996;100:468-71.
36. Norris D, Bawendi M. Measurement and assignment of the size-dependent optical spectrum in CdSe quantum dots. Phys Rev B 1996;53:16338-46.

37. Pons T, Lequeux N, Mahler B, Sasnouski S, Fragola A, Dubertret B. Synthesis of near-infrared-emitting, water-soluble CdTeSe/CdZnS core/shell quantum dots. Chem Mater 2009;21;1418-24.

38. Yang P, Wang S, Murase N, Near-infrared emitting $CdTe_{0.5}Se_{0.5}/Cd_{0.5}Zn_{0.5}S$ quantum dots: synthesis and bright luminescence. Nanoscale Res Lett 2012;7:615.

39. Yang P, Cao Y, Li X, Zhang R, Liu N, Zhang Y, $CdTe_{1-x}Se_x/Cd_{0.5}Zn_{0.5}S$ core/shell quantum dots: core composition and property. Luminescence 2014;29;407-11.

40. Liang G-X, Li L-L, Liu H-Y, Zhang J-R, Burda C, Zhu J-J, Fabrication of near-infrared-emitting CdSeTe/ZnS core/shell quantum dots and their electrogenerated chemiluminescence. Chem Commun 2010;46;2974-76.